Understanding target-like signals in coastal altimetry: Experimentation of a tomographic imaging technique

A. Scozzari,[1] J. Gómez-Enri,[2] S. Vignudelli,[3] and F. Soldovieri[4]

Received 4 November 2011; revised 20 December 2011; accepted 20 December 2011; published 20 January 2012.

[1] Usage and availability of Sea Surface Height (SSH) information from satellite radar altimeters undergo known limitations in the coastal zone, where such data are of great importance and usefulness. In fact, coastal regions are a crucial zone to be investigated and monitored, due to the high impact that sea level and circulation changes have on the environmental security and the related economic and societal issues. It is known that radar returns from the sea surface sometimes present target-like echoes ("bright targets"), especially in correspondence of particular features of the coastal zone, thus entailing a potential interference with the measurement of SSH. Such spiky echoes generate hyperbolic patterns in the radargram domain, which the recent literature has tentatively explained as resulting from flat water areas in the proximity of the coastline, but the physical mechanism that underlies their occurrence still remains unclear. To probe further into this aspect, this work describes a novel application of a microwave tomographic reconstruction approach, applied to the Envisat RA-2 signals, tested on selected passes over the Pianosa Island (a 10 km^2 island in the NW Mediterranean). The aim of this study is the analytical identification of the signal contamination sources in terms of location and extension of their associated electromagnetic anomaly. The obtained results confirm the idea that the origin of such signatures is connected with particular conditions of the sea surface, which are easier to be found in the proximity of coastal closed areas such as gulfs, but presumably not limited to such circumstances. **Citation:** Scozzari, A., J. Gómez-Enri, S. Vignudelli, and F. Soldovieri (2012), Understanding target-like signals in coastal altimetry: Experimentation of a tomographic imaging technique, *Geophys. Res. Lett.*, *39*, L02602, doi:10.1029/2011GL050237.

1. Introduction

[2] Radar altimetry is a remote sensing technique supporting the studies of sea level variability, including the rate of the global average rise in response to global warming. Measurements from radar altimetry have shown that the sea level is rising globally by about 3 mm/year since 1993, which is almost twice the rate estimated from tide gauges at coastal and island sites in the past century [*Church and White*, 2011]. These findings have the largest impact in the coastal zone, where approximately 75% of the world's population will live by 2025 [*Hinrichsen*, 1998]. However, the altimeter-derived estimates of the recent sea level rise are usually based on open ocean measurements and are not performed at the land-sea interface, where tide gauges are located. Therefore it is of primary importance, as recommended by *Cazenave et al.* [2010], to investigate the various factors (natural processes, instrumental bounds and data processing limitations) that may affect the correlation between altimetry measurements and tide gauge data.

[3] In this particular framework, coastal altimetry is a piece of the coastal sea level monitoring puzzle [*Fernandes et al.*, 2011] that promises to bring significant benefits to the integration between remotely sensed and in situ measurements. In fact, through the re-analysis of old archives and the application of newly developed processing schemes, it is possible to get closer to the coast in the extraction of meaningful information about the sea level. A foreseen outcome of such capability is the production of a new global coastal altimetry product [*Vignudelli et al.*, 2011a, 2011b].

2. Analysis of Signals From the Altimetric Satellite Platform

2.1. Sea Surface Height Information Contained in the Radar Altimeter Waveforms

[4] The radar altimeter is a nadir looking instrument located on a satellite platform, transmitting a sequence of radar pulses down to the Earth surface, and recording the raw waveforms associated with the returned echoes.

[5] An on-board tracking system keeps the reflected signal inside the time window of the recorded waveform, trying to tie the leading edge of the echo coming from the air-water interface to a specific location in the time domain. A successive processing step to retrieve geophysical information from the raw waveforms is performed on the ground and is called "retracking". The basic idea of retracking is to fit a particular model to the acquired waveform in order to retrieve the required geophysical parameters, such as the measurement of range. "Range" is defined as the distance between the satellite's centre of mass and the mean sea surface within the altimeter's footprint, and is connected with the time of the leading edge of the reflected signal. The estimation of range undergoes corrections for instrumental errors, atmospheric delays and ocean effects (i.e. Sea State Bias), which are performed in the ground processing chain. Finally, the corrected range is referred to the Earth reference ellipsoid, obtaining the Sea Surface Height (SSH) estimation. The procedure outlined here is well described by *Fu and Cazenave* [2001].

[6] Waveform retracking plays a key role in producing good SSH data. A suite of retracking algorithms has been

[1]Istituto di Geoscienze e Georisorse, Consiglio Nazionale delle Ricerche, Pisa, Italy.
[2]Applied Physics Department, University of Cadiz, Puerto Real, Spain.
[3]Istituto di Biofisica, Consiglio Nazionale delle Ricerche, Pisa, Italy.
[4]Istituto per il Rilevamento Elettromagnetico dell'Ambiente, Consiglio Nazionale delle Ricerche, Naples, Italy.

0094-8276/12/2011GL050237

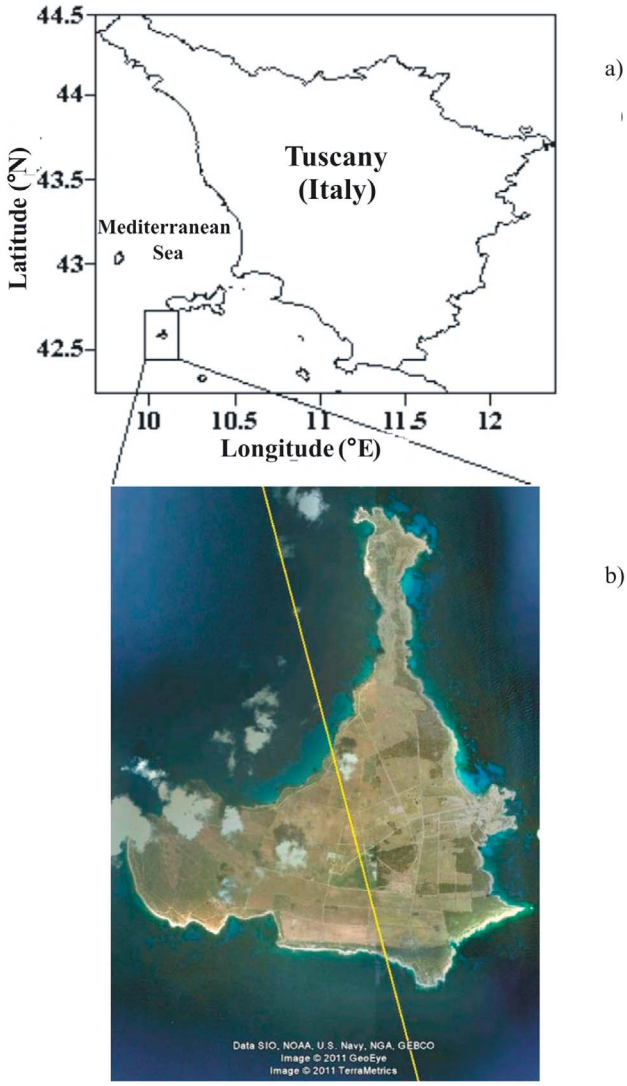

Figure 1. (a) Study area and (b) Pianosa Island. The yellow line shows the nominal route for Envisat orbit 128.

proposed, dealing with specific domains (i.e. open ocean, coastal zone, ice). Results till now have shown that there is still margin for improving the quality and availability of the information extracted from the raw altimetry waveforms [*Yang et al.*, 2010; *Gommenginger et al.*, 2011]. A necessary step in this direction can be done by the analysis of the physical and electromagnetic effects associated with particular features of such signals.

2.2. Target-Like Features in the Particular Case Study

[7] In this work, we use RA-2 altimeter data from the *European Space Agency* (ESA) Envisat mission, covering the period between 2002 and 2008. The revisit time of the satellite platform is 35 days. The radar system on board Envisat is designed to average 100 consecutive raw waveforms, thus providing range measurements at 18 Hz from a native PRF (Pulse Repetition Frequency) of 1800 Hz. The along-track spacing between two consecutively averaged waveforms is about 350 m.

[8] Typical footprints of radar altimeters have a radius of a few kilometres on the illuminated surface. The RA-2 pulse-limited footprint is in the range 1.7–10 Km, and its variability depends on the sea state [*Robinson*, 2004]. As a consequence, passages close to the coasts represent an issue to be specifically managed; in fact, the radar signal can be affected by reflections from land, vegetation and other objects that fall within the footprint [*Brooks et al.*, 1998]. Even flat surfaces (such as the case of quasi-calm sea or flooded areas) can lead to deviations of the received signals from the "Brown" model [*Brown*, 1977], which is the waveform model generally used for the estimation of SSH in open-ocean conditions.

[9] *Gómez-Enri et al.* [2010] showed an intermittent and apparently unpredictable contamination pattern affecting the data acquired in the coastal zone. Authors analyzed a series of waveforms taken from an Envisat track crossing the Pianosa Island in the Tuscan Archipelago (Northwestern Mediterranean). Almost one third of the cases exhibited a particular pattern in the resulting radargrams, which consisted in a strong bright return of hyperbolic shape. Various alternative sources of such observed feature have been discussed, and it was suggested that the phenomenon is due to calm waters, but the mechanism which triggers this condition is still unclear.

[10] Moving forward from this point, this work introduces the usage of a target focusing method, experimented on Envisat RA-2 datasets. The fundamental idea is to help individuating the location and extent of the source of the hyperbolic patterns, for a better understanding of the mechanisms underlying such phenomena.

[11] Pianosa is a small island (10 km^2) belonging to a marine regional park (Parco nazionale dell'Arcipelago Toscano) in front of the coasts of Tuscany (Figure 1a), which is mostly characterised by flat and dry land (Figure 1b). Both the land and the typical vegetation that covers the island are expected to be a weak radar reflector for RA-2 signals [*Long*, 2001]. Also, interdiction of private navigation in the area reduces the possibilities of echoes from vessels.

[12] In addition, Pianosa has a favourable intersection with Envisat passes. In particular, the ascending orbit numbered 128 crosses Pianosa Island and its Golfo della Botte, which has been previously identified as an interesting site for the assessment of non-Brown returns [*Gómez-Enri et al.*, 2010]. All these aspects make this site an excellent location to understand particular patterns at the land-sea interface.

3. Target Focusing Method

[13] Focusing of the reflecting targets is achieved by a tomographic reconstruction approach, in order to obtain a reliable estimation of their location and extent. The reconstruction approach falls within the inverse scattering techniques [*Colton and Kress*, 1992] and permits to detect and localize targets in terms of "electromagnetic anomalies" with respect to a background scenario. In this specific case, the background is given by a homogeneous free-space medium, and anomalies correspond to high values of the contrast function. The synthetic aperture ensured by the large footprint of the altimeter makes it possible to see the target from different antenna spatial points, allowing the tomographic approach to deliver a focused image of the target.

[14] Here, we assume a 2D geometry, with the (x–z) plane taken as investigation plane and with a background scenario represented by the free space medium, where the electromagnetic wave propagates before to impinge on the reflecting target. The x-axis corresponds to the along-track direction and the z-axis corresponds to the zenith direction.

[15] The contrast function is defined as the difference between the equivalent dielectric permittivity of the target and the one of the free space. The only a priori information required by the inversion approach regards the investigation domain D, within which the contrast function is searched for. For the problem at hand, the 2D investigation domain is given as a rectangle $D = [-a.a] \times [z_{\min}, z_{\max}]$. The term a represents the semi-extent of the investigation domain D along the x-axis, whereas its height (depth) spans an interval from $z_{\min}$ to $z_{\max}$ that contains the sea-air interface, assumed at depth z = 0.

[16] The datum of the problem is given as the field scattered by the reflecting target after transformation to the frequency domain. Here, we exploit a linear inverse scattering approach that is achieved under a simplified scattering model, known as "Born Approximation" [*Soldovieri and Solimene*, 2010]. Born Approximation neglects the mutual electromagnetic interactions among the targets that are in the scene. This simplified hypothesis is particularly suitable for the cases at hand, where the targets in the scene are few and well spaced, making mutual interactions reasonably negligible. Further details about this technique are provided in the auxiliary material.[1]

[17] Under Born Approximation, a linear integral equation relates the contrast function to the scattered field; the kernel of such an integral equation accounts for the incident field propagating from the altimeter antenna (transmitting) to the target and the trip back from the target to the receiving antenna on the altimeter.

[18] The above considerations can be made explicit from a mathematical point of view by writing the integral equation that has to be solved [*Soldovieri and Solimene*, 2010], as

$$E_s(\omega, x_s, z_s) = k_0 \int_{z_{\min}}^{z_{\max}} \int_{-a}^{a} \frac{\chi(x', z')}{R} e^{-j2k_o R} dx' dz' \qquad (1)$$

where a scalar factor outside of the integral has been omitted, and where $E_s(\omega, x_s, z_s)$ is the datum of the problem, i.e., the scattered field collected at pulsation $\omega = 2\pi f$, (f is the working frequency) and at the spatial location (x_s,z_s) of the altimeter; k_0 is the wavenumber in the free space, $R = \sqrt{(x_s - x')^2 + (z_s - z')^2}$ is the distance between the altimeter and the generic point of the investigation domain. The contrast function $\chi(x', z')$ is the unknown of the problem and is defined as the following a-dimensional quantity:

$$\chi(x', z') = \frac{\varepsilon(x', z')}{\varepsilon_0} - 1 \qquad (2)$$

where $\varepsilon_{eq}(x', z')$ is the (unknown) equivalent permittivity function of the target, given as $\varepsilon_{eq}(x', z') = \varepsilon(x', z') + \frac{\sigma(x', z')}{j\omega}$, where $\varepsilon(x', z')$ and $\sigma(x', z')$ are the dielectric permittivity and conductivity of the target, respectively; ε_0 is the dielectric permittivity of the free space medium.

[19] After the discretization of the integral equation, the problem can be formulated as a matrix inversion problem in the following form:

$$\underline{E}_s = \underline{\underline{A}}\,\underline{\chi} \qquad (3)$$

where $\underline{\underline{A}}$ is a matrix arising from the discretization of the integral equation (1), which is achieved by the method of moments [*Harrington*, 1961]; $\underline{E}_s$ is the stacked data vector made of the M·N elements, where N represents the number of spatial points (i.e. the number of waveforms acquired at 18 Hz rate) and M is the number of working frequencies; $\underline{\chi}$ represents the discretization of the contrast function (2) in the investigation domain and is represented as a vector made up of the P pixellated values of the contrast function in the investigation domain D. In particular, the investigation domain D is discretized by rectangular pixels with extent Δx, Δz along the x- and z-axis respectively. Therefore, the matrix A has dimension (M·N) × P, with M·N rows and P columns.

[20] With the aim to counteract the possible ill-conditioning of the inverse problem, the inversion of the matrix relation (3) is performed by means of the Truncated Singular Value Decomposition (TSVD) [*Bertero*, 1989], which is a regularization scheme used to achieve a stable solution; the inversion provides the bi-dimensional spatial map (in the along-track and zenith directions) of the contrast function $\chi(x', z')$ in the investigation domain D. Finally, the reconstruction result is given as the modulus of the contrast function, where the regions characterised by a significant modulus are representative of the targets' location and geometry.

[21] It is worth noting that the inversion approach works in the frequency domain. Under the hypothesis that the scattered field is proportional to the instantaneous waveform amplitude, the collected altimeter waveforms undergo a Fourier transform, so to obtain, for each spatial measurement, the scattered field in the frequency domain.

4. Data Selection and Processing

[22] We analysed Envisat RA-2 waveforms covering the period between 13 November 2002 (cycle 11) and 30 April 2008 (cycle 68), extracted from the ESA Sensor Geophysical Data Records (SGDR) product. Available data during the studied period regarded 53 cycles. A data subset across the Pianosa Island has been extracted from the ascending orbit number 128. It consists of 50 waveforms of consecutively returned signals, with the island kept approximately in the middle (Figure 1b).

[23] For the tomographic reconstruction, waveforms were organized as a B-scan (an aligned set of in-depth measurements to perform a cross-sectional visualisation) with 50 spatial observation points (one per each acquired waveform) spaced by an along-track distance of 350 m. Each waveform is made up of 128 samples with a time step of 3.125 ns, which corresponds to the gate width of the 320 MHz chirp signal of the RA-2 in Ku band.

[24] The air-sea interface (also known as *Tracking Point*) is assumed to be at the 47th time sample, being the nominal tracking point defined by ESA at gate number 46.5 [*Gommenginger et al.*, 2011]. Then, each waveform undergoes

[1] Auxiliary materials are available in the HTML. doi:10.1029/2011GL050237.

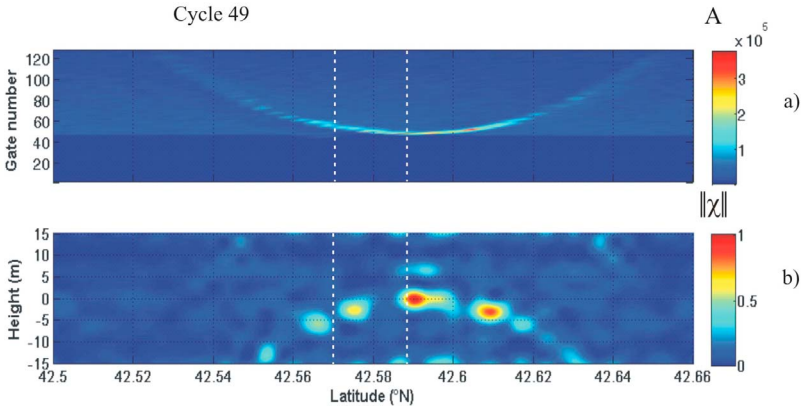

Figure 2. (a) Radargram and (b) tomographic reconstruction of the studied portion of track 128 in cycle 49. The instantaneous amplitude (A) of radargram waveforms (Figure 2a) is given in terms of digitised counts number. Tomographic reconstruction (Figure 2b) is given in terms of modulus of the normalised contrast function ($\|\chi\|$). Axes show the along-track positioning (expressed in latitude) and height with respect to the nominal air-sea interface (in meters); dashed white lines identify the island boundaries.

a Fourier Transform, and the information is arranged in M = 21 uniformly spaced frequencies in the working band [13.4, 13.5] GHz.

[25] The observation domain (i.e. the portion of space where the scattered field is measured) is made up of the 50 spatial observation points, placed at height z_s (nominal orbit altitude of the altimeter). The investigation domain D, where to search for the contrast function (representative of the target), has an extent of $2a$ = 17150 m along the x-axis, which is equal to the one of the observation domain, while along the z-axis it spans the limited interval [$z_{min} = -15$, $z_{max} = 15$] m and is centered with respect to the air/sea interface located z = 0. The choice of a 30 meters wide interval along the z-axis represents a good tradeoff between computational cost and affordability of the result, by guaranteeing that the target falls within the investigation domain.

[26] The investigation domain is discretized at a step Δx = 350 m, Δz = 3 m; in particular, the step along the x-axis is chosen equal to the measurement step (observation), whereas the step Δz is comparable with the resolution limits imposed by the working band used in the inversion (put equal to 100 MHz).

[27] Inversion of the matrix is carried out by the TSVD scheme, where only the singular values larger than 0.1 times the maximum value are retained in the TSVD expansion.

5. Results and Discussion

[28] Examination of the 53 available cycles revealed a bright target, denoted by a hyperbolic feature in the radargram, in about 30% of the satellite passes over Pianosa. Further selection of cycles has been done, based on the true satellite course crossing the island. Cycles 27, 49 and 51 have been chosen thanks to their substantially overlapped footprints, a necessary condition to reduce the possibility that different results may be due to particular land features seen from different angles. In fact, the cross-track distance between the selected orbits is less than 500 m. Figure S1 in the auxiliary material shows a topographic map of Pianosa (derived from a Digital Elevation Model), overlapped by the true satellite orbits for the selected cycles.

[29] Radargrams and tomographic reconstructions for cycles 49 and 51 of orbit 128 are presented in Figures 2 and 3, respectively. Figures 2a (cycle 49) and 3a (cycle 51) show hyperbolic features in the radargram domain, which are characterised by the apex located at the air-sea interface. Both tomographic images (Figures 2b and 3b) exhibit contrast function anomalies at the north of the island that, after focusing, assume the shape of two reflective targets; in both cases, one target appears just attached to the coastline, while the other one is placed further from the coast. The average dimension of the focused targets along the x-axis is about 450 m; the distance of the furthest target from the coast, calculated by projecting the retrieved contrast function modulus on the true satellite orbits, is about 2.3 Km.

[30] A remarkable fact is that, in both cycles, the closest anomalies to the coast have a reconstructed depth falling in the bin around z = 0, as determined in the discretized domain defined in Section 4. This peculiarity, together with their particular location, assigns such targets to the air-sea interface region, in an area just next to the coastline.

[31] Figure 4a shows the radargram resulted from the analysis of cycle 27, where a strong hyperbolic pattern is evident, in the form of a wide target-like overpeaking with respect to the typical Brown return. It should be noted that the apex of such hyperbolic feature is above the air-sea interface in the radargram domain, thus revealing an off-track reflector responsible for the observed strong burst.

[32] The tomographic reconstruction (Figure 4b) points out a relatively wide anomaly (in terms of its along-track span) of the contrast function at the north of the island. The target appears to be extended for about 1.5 Km in the along-track direction. The maximum modulus of the contrast function is located at about 1.1 Km off the island (in the along-track direction) at an apparent depth z = −6 m, which identifies the anomaly at about 3.2 Km off the center of the footprint, under the hypothesis that the target lies on the air-sea interface. This is coherent with the off-track position assessed by the observation of the radargram.

[33] Alternative sources connected with terrain structures or floating vessels can hardly be responsible for such strong return. In fact, an eventual flat land surface oriented normal

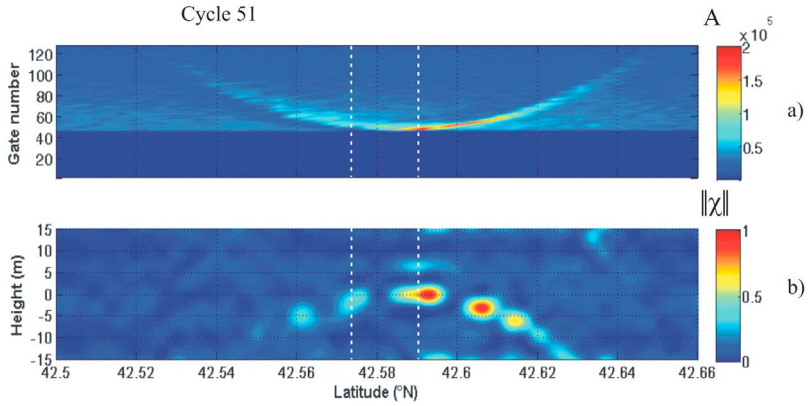

Figure 3. Same diagrams as for Figure 2, concerning cycle 51.

to the line of sight would generate a permanent strong nadir backscatter; particular moisture conditions can actually modulate such intermittent effect, but the absence of particular rain events preceding the satellite passages lead to the exclusion of this eventuality. Last, there are no sufficiently wide corner reflectors to justify the strong signal, due to the relevant extension in length of the reconstructed target (and the wideness in time of its related echo in cycle 27). Also, an eventual land scatterer is very unlikely to be responsible for the observed behaviour. In fact, the strong target-like echo does not appear in adjacent cycles like 50 (which passes about 18 m far from cycle 27), implying an extreme directionality of such scatterer in the across-track direction. The same scatterer should be sufficiently isotropic in the along-track direction to return a strong echo all over the covered piece of the radargram (about 15 Km), such as it does in all the cases where the hyperbolic pattern appears.

[34] Figure 5 shows the location of the individuated reflective zones, obtained by projecting the maximum modulus of the contrast function along the zenith direction (z-axis) on each point of the satellite track. It is clearly shown how the anomalies are systematically located inside the shoreline of the Golfo della Botte, at the north of the island.

[35] *Long* [2001] offers a deep analysis of surface effects in radar returns, by exploring the behaviour of both land and sea surfaces. Target-like echoes in radar observations of the ocean surface are reported to be caused by very local phenomena, such as unbroken wave crests and white caps, but also by calm water circumstances, that may regard relatively large areas.

[36] It is thus understandable how this kind of phenomena, which is occurring with appreciable frequency in our particular study area, may arise wherever such conditions are met, even in the open sea. This latter aspect gives a high importance to this study, and suggests moving forward with the analysis of altimetry datasets featured by bright target effects, for a better understanding of the underlying mechanisms even outside the coastal context.

6. Conclusions

[37] Pianosa Island represents an effective site for benchmarking methods to better understand the triggering mechanisms of target-like responses in radar altimetry measurements. In particular, target-like features in the collected waveforms can potentially alter the derived SSH estimation. Past tentative explanations of these phenomena identified their origin in flat water areas in the proximity of the coastal zone.

[38] The application of an assessed tomographic technique to this specific context enhances the analytical possibilities available for this kind of investigation, by providing

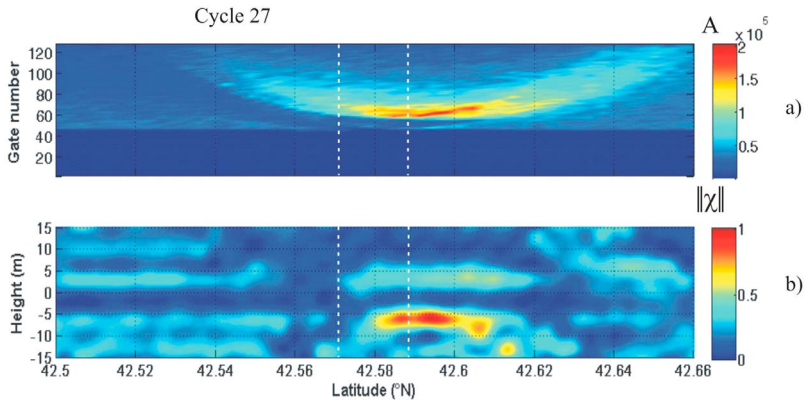

Figure 4. Same diagrams as for Figure 2, concerning cycle 27.

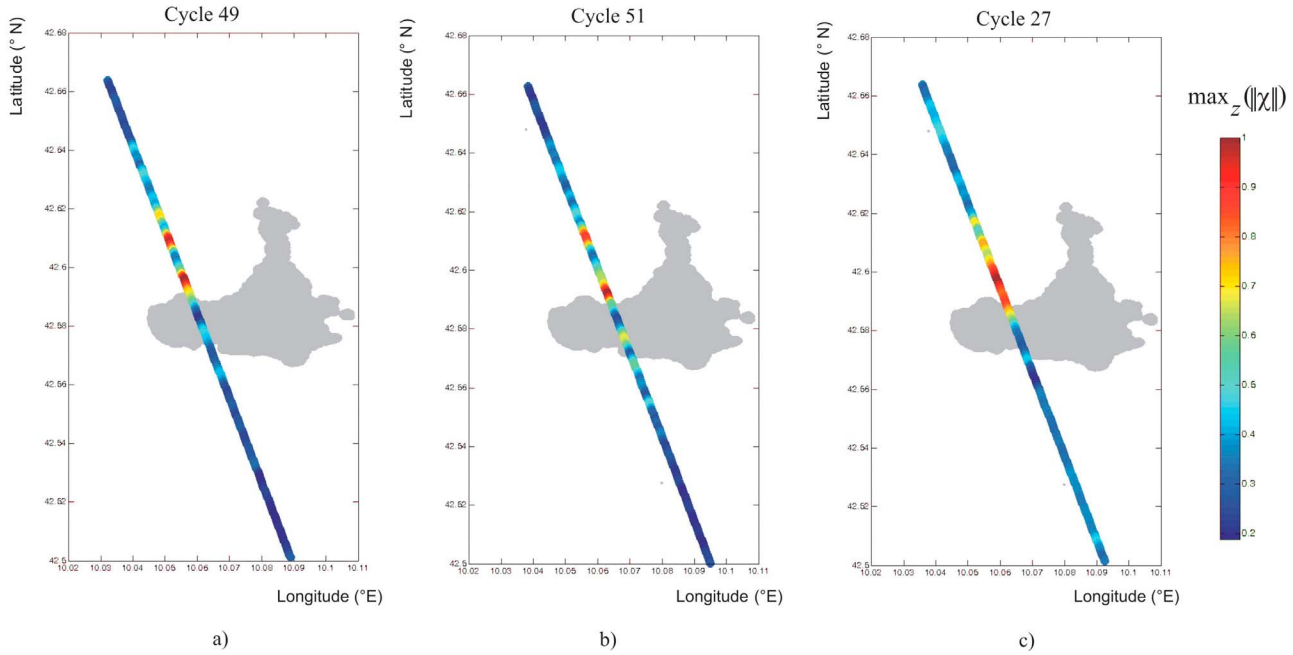

Figure 5. Projection of the maximum modulus of the contrast function along the zenith direction for each point of the satellite pass (track 128) for (a) cycle 49, (b) cycle 51, and (c) cycle 27.

information on the location and extent of the detected electromagnetic anomalies (targets) in the investigated scenario.

[39] Results of this work confirm and reinforce the hypothesis that bright targets are connected with particular sea state circumstances, such as unbroken wave crests, white caps, and calm water areas. These results suggest further investigations of altimetry datasets featured by bright target effects, including data gathered in the open ocean, which is not necessarily immune from such conditions. Moreover, the tomographic reconstruction can contribute to a novel approach in the retracking procedures, especially when dealing with altimetry datasets potentially affected by target-like effects. In particular, the reconstruction technique can support the localization of anomalous targets and the subsequent adaptation of the retracking procedure to the conditions detected, opening the possibility to a new conceptual scheme for the extraction of the geophysical information from radar altimetry signals.

[40] **Acknowledgments.** Data used for the preparation of this work have been provided in the framework of the ESA "COASTALT" project (ESA-ESRIN contract 20698/07/I-LG), to which the authors are deeply grateful. Acknowledgments go also to the Spanish Ministry of Education and Science (project CGL2008-04736) for contributing to the activity.

[41] The Editor thanks Lorenzo Lo Monte and an anonymous reviewer for their assistance in evaluating this paper.

References

Bertero, M. (1989), Linear inverse and ill-posed problems, in *Advances in Electronics and Electron Physics*, vol. 75, edited by P. W. Hawkes, pp. 1–120, Academic, New York.

Brooks, R. L., D. W. Lockwood, J. E. Lee, D. W. Handcock, and G. S. Hayne (1998), Land effects on TOPEX radar altimeter measurements in Pacific Rim coastal zones, in *Remote Sensing of the Pacific by Satellites*, edited by R. A. Brown, pp. 175–198, Earth Ocean and Space, Glebe, Australia.

Brown, G. S. (1977), The average impulse response of a rough surface and its applications, *IEEE Trans. Antennas Propag.*, *25*(1), 67–74, doi:10.1109/TAP.1977.1141536.

Cazenave, A., D. P. Chambers, P. Cipollini, L. L. Fu, J. W. Hurrell, M. Merrifield, S. Nerem, H. P. Plag, C. K. Shum, and J. Willis (2010), Sea level rise - Regional and global trends, in *Proceedings of OceanObs'09: Sustained Ocean Observations and Information for Society*, vol. 1, *ESA Publ. WPP-306*, pp. 11, edited by J. Hall, D. E. Harrison, and D. Stammer, Eur. Space Agency, Frascati, Italy, doi:10.5270/OceanObs09.

Church, J. A., and N. J. White (2011), Sea-level rise from the late 19th to the early 21st century, *Surv. Geophys.*, *32*(4–5), 585–602, doi:10.1007/s10712-011-9119-1.

Colton, D., and R. Kress (1992), *Inverse Acoustic and Electromagnetic Scattering Theory*, Springer, Berlin.

Fernandes, M. J., J. Benveniste, and S. Vignudelli (2011), Improved coastal altimetry could contribute to the monitoring of regional sea level trends, *Eos Trans. AGU*, *92*(16), 136, doi:10.1029/2011EO160004.

Fu, L. L., and A. Cazenave (Eds.) (2001), *Satellite Altimetry and Earth Sciences; A Handbook of Techniques and Applications*, Academic, San Diego, Calif.

Gómez-Enri, J., S. Vignudelli, G. D. Quartly, C. P. Gommenginger, P. Cipollini, P. G. Challenor, and J. Benveniste (2010), Modeling Envisat RA-2 waveforms in the coastal zone: Case-study of calm water contamination, *IEEE Geosci. Remote Sens. Lett.*, *7*(3), 474–478, doi:10.1109/LGRS.2009.2039193.

Gommenginger, C., P. Thibaut, L. Fenoglio-Marc, G. D. Quartly, X. Deng, J. Gómez-Enri, P. G. Challenor, and Y. Gao (2011), Retracking altimeter waveforms near the coasts, in *Coastal Altimetry*, edited by S. Vignudelli et al., pp. 61–101, Springer, Berlin, doi:10.1007/978-3-642-12796-0_4.

Harrington, R. F. (1961), *Time-Harmonic Electromagnetic Fields*, McGraw-Hill, New York.

Hinrichsen, D. (1998), *Coastal Waters of the World: Trends, Threats and Strategies*, Island, Washington, D. C.

Long, M. W. (2001), *Radar Reflectivity of Land and Sea*, Artech House, Boston.

Robinson, I. S. (2004), *Measuring the Oceans From Space: The Principles and Methods of Satellite Oceanography*, Springer, Berlin.

Soldovieri, F., and R. Solimene (2010), Ground penetrating radar subsurface imaging of buried objects, in *Radar Technology*, edited by G. Kouemou, pp. 105–126, InTech, Rijeka, Croatia.

Vignudelli, S., et al. (2011a), Satellite altimetry: Sailing closer to the coast, in *Remote Sensing of the Changing Oceans*, edited by J. Gower et al., pp. 217–238, Springer, Berlin, doi:10.1007/978-3-642-16541-2_11.

Vignudelli, S., A. G. Kostianoy, P. Cipollini, and J. Benveniste (Eds.) (2011b), *Coastal Altimetry*, Springer, Berlin, doi:10.1007/978-3-642-12796-0.

Yang, L., M. Lin, Q. Liu, and D. Pan (2010), Retracking strategy based on waveform classification and subwaveform extraction for coastal altimetry

along China coastal seas, in *Proceedings of IGARSS 2010*, pp. 632–635, Inst. Electr. and Electr. Eng., Honolulu, 25–30 July, doi:10.1109/IGARSS.2010.5653203.

J. Gómez-Enri, Applied Physics Department, University of Cadiz, Av. Republica Saharaui, s/n 11510 Puerto Real (Cadiz), Spain.

A. Scozzari, Istituto di Geoscienze e Georisorse, Consiglio Nazionale delle Ricerche, Via Moruzzi 1, I-56124 Pisa, Italy. (a.scozzari@igg.cnr.it)

F. Soldovieri, Istituto per il Rilevamento Elettromagnetico dell'Ambiente, Consiglio Nazionale delle Ricerche, Via Diocleziano 324, I-80124 Naples, Italy.

S. Vignudelli, Istituto di Biofisica, Consiglio Nazionale delle Ricerche, Via Moruzzi 1, I-56124 Pisa, Italy.